MALAYSIAN JOURNAL OF ANALYTICAL SCIENCES

Journal homepage: https://mjas.analis.com.my/

Research Article

Adsorption of phosphorus onto raw hard clam shell through up-flow column reactor using synthetic water

Norzainariah Abu Hassan[1*], Nur Aleya Muhamad Imran Wong[2], Nursyazana Mohd Nor[2], Muhamad Saiful Airell Eddy[2], Sivasini Saravanan[2], Muhammad Danish Farhan Mohamad Adli Azdhar[2], Annclare Supang Apoi[2], Noorul Hudai Abdullah[2*], Nur Husna Muslim[1], and Nur Syazrena Amyza Zainal[3]

[1]Faculty of Engineering Technology, Universiti Tun Hussein Onn Malaysia, Pagoh Education Hub, 84600 Pagoh, Johor, Malaysia
[2]Neo Environmental Technology, Centre for Diploma Studies, Universiti Tun Hussein Onn Malaysia, Pagoh Education Hub, 84600 Pagoh, Johor, Malaysia
[3]Multi Tank Terminal Sdn Bhd, PT 64374, Jalan Perigi Nenas 8/8, Taman Perindustrian Pulau Indah, Pulau Indah, Westport, 42920 Pelabuhan Klang, Selangor`

[*]Corresponding author: zainariah1077@gmail.com; noorul@uthm.edu.my

Received: 15 September 2025; Revised: 19 January 2025; Accepted: 22 January 2026; Published: 28 February 2026

Abstract
Phosphorus pollution in aquatic ecosystem is a critical environmental issue due to its direct contribution to eutrophication, algal blooms, and subsequent deterioration of water quality. Conventional methods of phosphorus removal are costly and generate secondary environmentally impacts necessiting the exploration of sustainable alternatives. This study investigates the potential of raw hard clam shells as a low-cost and eco-friendly adsorbent for phosphorus removal using an up-flow column reactor with synthetic water. Six up-flow column reactors were operated at constrant flow rates with varying bed depths (1, 2, 3, 4, 6, and 8cm) to evaluate adsorption performance. Experimental findings demonstrated that raw hard clam shells possess significant phosphorus adsorption capacity. The maximum adsorption capacity and rate-controlling mechanisms were elucidated through the application of Bed Depth Service Time, Modified Mass Transfer, and Thomas models. The physical-chemical characteristics and morphological changes of the adsorbent before and after adsorption were systematically examined. Operational studies indicated that optimal removal efficiency was achieved at specific flow rates and contact times, emphasizing the importance of reactor configuration and operating conditions. Overall, this findings highlight the effectiveness and sustainability of raw hard clam shells as a natural adsorbent for phosphorus removal from synthetic water in continuous flow systems.

Keywords: phosphorus, raw hard clam shell, bed depth service time, modified mass transfer, Thomas model

Introduction

In aquatic systems, phosphorus, primarily present as phosphate (PO_4^{3-}), function as an essential nutrient; however, excessive concentration can trigger severe ecological disturbances. Elevated phosphate levels accelerate eutrophication, promoting the proliferation of aquatic plants and algae blooms which subsequently deplete dissolved oxygen (DO), destabilize aquatic ecosystems, and deteriorate water quality [1,2]. These processes can ultimately result in the collapse of aquatic biodiversity. Consequently, stringent regulation of phosphorus discharge control, particularly from point sources such as municipal and industrial wastewater, is critical to sustaining ecosystem integrity. While many developed countries have adopted stricter effluent standards such as the US Environmental Protection Agency (USEPA) and the European Union (EU) Wastewater Directive, which restrict total phosphorus (TP) concentrations to 0.8 mg/L and 2 mg/L, respectively. In Malaysia, the Environmental Quality (Sewage and Industrial Effluent) Regulations 2009 prescribe phosphorus discharge limits under Standard A and Standard B classifications. For inland water bodies, Standard B permits phosphorus concentrations of up to 10 mg/L, whereas the more stringent Standard A restricts discharge levels to a maximum of 5 mg/L [3,4]. Enhancing phosphorus control in Malaysia necessitates a multifaceted approach, including the establishment of more stringent regulatory standards, the upgrading of wastewater treatment infrastructure, the promotion of sustainable agricultural practices and

the public awareness initiatives. Additionally, providing economic incentives for industries and farmers to adopt phosphorus-mitigation strategies could further accelerate the reduction of nutrient discharges and support long-term water quality management.

Phosphate removal from wastewater can be accomplished through a variety of physical, chemical, and biological methods, each with distinct advantages and limitations. Biological treatment, in particular, offers a cost-effective and environmentally sustainable option; however, its efficiency is highly sensitive to operational parameters. Effective performance requires strict regulation of the carbon-to-phosphorus ratio, sludge retention time, and the alternation of anaerobic–aerobic conditions [5]. In practice, maintaining these conditions consistently can be challenging, especially in decentralized or resource-limited treatment systems, thereby constraining the reliability of biological approaches compared with more robust chemical or physical-chemical alternatives. Although chemical precipitation with iron or aluminium salts is widely applied, it increases operating costs and generates chemical sludge that requires further handling and disposal [6]. In comparison with other alternative and commercial phosphate adsorbents, calcium-based shell materials exhibit moderate but competitive removal performance while offering clear advantages in terms of cost, availability, and environmental sustainability. Commercial adsorbents such as iron-based media and activated alumina commonly achieve higher phosphate removal efficiencies due to their high surface area and chemically engineered active sites. However, these materials are typically associated with higher production costs, complex synthesis procedures, and secondary waste generation [7,8]. In contrast, shell-derived calcium carbonate adsorbents, including egg, oyster, and mussel shells, have demonstrated removal efficiencies ranging from 30 – 80%, depending on modification method and operational conditions, with phosphorus removal governed primarily by calcium-phosphate precipitation and surface complexation mechanism [9,10]. Although unmodified shell materials generally exhibit lower surface area than commercial adsorbent, their effectiveness in phosphate removal is well documented, particularly in treatment systems emphasizing sustainability and low operational cost [7]. Accordingly, the present study demonstrates the feasibility of utilising raw hard clam shells as an unmodified, waste-derived adsorbent in a continuous up-flow column system, providing a practical baseline for further optimisation and potential large-scale application.

Compared to batch adsorption systems, column adsorption provides closer representable of actual water treatment practices. In particular, up-flow column reactors offer several advantages, including improved hydraulic flow distribution, reduced risk of clogging, and extended contact time between adsorbent and water. However, there is a clear research gap concerning the application of raw, unmodified clam shells under comparable hydrodynamic conditions. Previous investigations have primarily focused on phosphate adsorption using iron-coated shells in hybrid plug-flow columns [11], yet limited work has addressed the performance of unmodified clam shells in controlled synthetic water systems with defined phosphorus concentrations. Accordingly, this study employs an up-flow column reactor to evaluate the effectiveness of raw hard clam shells as a sustainable natural adsorbent for phosphorus removal from synthetic water. The primary objectives are to investigate removal efficiency, adsorption kinetics, and breakthrough behaviour under varying operational parameters, such as influent concentration and bed height. Experimental findings are further validated using Bed Depth Service Time (BDST), Modified Mass Transfer, and Thomas models to understand the rate-controlling mechanisms in the up-flow column reactor. Complementary characterisation of the physical-chemical characteristics and morphological transformations of the adsorbent before and after provides additional insight. This integrated approach contributes to the advancement of cost-effective and environmentally sustainable phosphorus removal technologies, with particular relevance for decentralised wastewater treatment applications in developing regions.

Materials and Methods

Synthetic solution

For the experimental procedures, a phosphate stock solution was prepared in the laboratory using potassium dihydrogen phosphate (KH_2PO_4) dissolved in deionised water. A concentration of 100 mg/L phosphate (PO_4^{3-}) was obtained by accurately weighing 0.1433 grams of KH_2PO_4 and dissolving it with 1 L of deionised water. This stock solution was subsequently diluted to approximately 10 mg/L to simulate phosphorus concentration corresponding to Standard B under the Malaysian Environmental Quality (Sewage and Industrial Effluents) Regulations 2009. The target concentration for the experimental runs were achieved through serial dilution of the stock solution, with the required dilution volumes calculated according to Equation (1).

$$M_1V_1 = M_2V_2 \quad (1)$$

Equation 1 was applied to calculate the volume of a stock solution (V_1) required to obtain the desired concentration and volume diluted solution. In this study, the initial concentration (M_1) of the stock solution is 100 mg/L, while the final concentration (M_2) was adjusted to 10 mg/L, with a total dilution volume (V_2) of 1000 mL. Maintaining phosphate

(PO_4^{3-}) concentration at approximately 10 mg/L was essential to ensure accuracy and consistency in the subsequent phosphorus analysis, which was performed using the reactive orthophosphate Amino Acid Method via HACH DR1900 spectrophotometer.

Adsorbent

The preparation of raw hard clamshell adsorbents is a critical step in determining their adsorption efficacy, with implications for both experimental accuracy and potential industrial applications. Following collection of the raw hard clam shells, the shells were thoroughly washed with tap water and repeatedly rinsed with deionised water to remove adhering dirt and surface impurities. The cleaned shells were then subjected to a two-stage drying process; initial sun-drying for several days to remove bulk moisture, followed by an oven drying at 30°C for 48 hours to ensure uniform and controlled dehydration. Adequate drying is essential, as residual moisture can occupy active adsorption sites and diminish adsorptive performance. The dried clamshells were subsequently crushed and ground using a mechanical mill, a process that increases surface area and enhances the availability of adsorption sites by facilitating more contact points between the adsorbent and the adsorbate. The ground material was then sieved to obtain particles sized within the 1.18 mm – 2.36 mm range, which provides a balance between sufficient surface area for adsorption and minimal drop in packed bed column systems. Finally, the prepared clamshell adsorbents were stored in sealed containers to prevent moisture reabsorption and contamination, thereby preserving their structural integrity and adsorption efficiency prior to experimental application.

Column operational studies

Up-flow column studies employing raw hard clam shells provide critical insights into the material's performance for phosphorus removal from aqueous solutions under continuous flow conditions. In this configuration, the column is filled with raw hard-shell particles, while synthetic water is introduced in an upward direction to maximize interaction between the adsorbent and the contaminant. Previous studies have demonstrated that operational parameters, including flow rate, bed height, and initial phosphorus concentration, exert a substantial influence on adsorption behaviour and breakthrough characteristics [12]. Specifically, increasing bed depth prolongs breakthrough time and enhances adsorption capacity, whereas higher flow rates generally reduce both. The adsorption efficiency of raw hard clam shells is further governed by physical-chemical attributes such as surface area, pore structure, and the abundance groups capable of binding phosphorus. Collectively these findings contribute to the optimisation of design and operating conditions while underscoring the potential of raw hard clam shells as a low-cost, sustainable adsorbent for phosphorus removal in wastewater treatment applications.

Figure 1 presents the schematic of the up-flow column reactor system employed in this study. Six up-flow columns were operated simultaneously under identical influent concentration and constant flow conditions, with bed depth as the sole varying parameter. Synthetic phosphorus-containing influent stored in a tank was delivered to the system via a peristaltic pump, which maintained a steady and controlled flow rate to ensure stable operating conditions throughout the experiment. The influent was introduced in an upward flow through six parallel columns packed with raw hard clam shells at bed depth of 1cm, 2 cm, 3 cm, 4 cm, 6 cm, and 8 cm, while the column diameter was fixed at 2.5 cm. Effluents from each column was collected separately at the outlet, allowing time-dependent monitoring of phosphorus concentrations. This multi-column configuration enables direct evaluation of the effects of bed depth on adsorption performance, breakthrough behaviour, and hydraulic retention time (HRT). The arrows in the diagram indicate the direction of water flow from the influent tanker through the peristaltic pump, into the columns, and finally to the effluent collection containers. **Table 1** summarises the design and operational characteristics of the up-flow column reactor system used for phosphate removal by raw hard clam shells adsorbent.

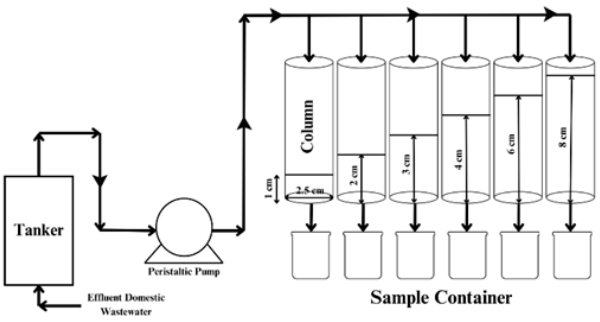

Figure 1. Schematic diagram of the up-flow column reactor

Table 1. Dimension of the up-flow column reactor treatment system

Parameter	Unit	Dimension
Hydraulic retention	h	0.584
Volumetric flow rate	L h^{-1}	0.1933
Column height	cm	23 cm
Internal diameter	cm	2.5 cm
Column material	-	Acrylic
Bed height	cm	1, 2, 3, 4, 6, 8
Amount of RHCS in the up-flow column reactor	g	7.785, 15.341, 23.751, 31.835, 45.269, 63.316
Particle size range	mm	1.18 to 2.36
Type of pump	-	Masterflex peristaltic pump

The performance of the up-flow column reactor was assessed by monitoring pH and phosphorus concentration at both the influent and effluent points of the system throughout a 14-days experimental period. Samples from each column are analysed immediately after the sample container is filled with half of the effluent to ensure precise data on phosphate removal. Each sample is filtered, and pH measurements are conducted using HANNA pH Benchtop Meters. Subsequently, samples from each column are analysed using the amino acid method and a HACH DR6000 Spectrophotometer to determine the concentration of retained phosphate by measuring the intensity of light passing through the samples. All column experiments were conducted in triplicate, and the reported results represent averaged values to ensure reproducibility and data reliability.

Analytical methods

The physical and chemical characteristics of an adsorbent govern its behaviour and interactions in both physical and chemical contexts, thereby influencing its composition, reactivity, and environmental impact. In phosphorus (PO_4^{3-}) adsorption studies, it is particularly important to evaluate these characteristics through X-ray Diffraction (XRD) analysis conducted both before and after the adsorption process. XRD provides critical insights into structural and compositional modifications, including the formation of new phosphate-containing crystalline phases and changes in crystallinity, both of which directly affect reactivity and adsorption capacity. By correlating XRD results with physical and chemical properties, researchers can elucidate the relationship between structural transformations and functional performance such as adsorption, catalysis, or dissolution. In this study, XRD analysis was performed at the Materials Physics Laboratory, while further analysis was carried out at Mint-SRC.

Scanning Electron Microscopy (SEM) was employed to capture high-resolution images of the adsorbent surface morphology, providing detailed characterization of topography, texture, and particle size both before and after phosphate adsorption. SEM images revealed the original surface characteristics of the material, including particle size and surface texture. Complementary to this, Energy-Dispersive X-Ray Fluorescence (EDXRF) was utilized as a non-destructive analytical technique to determine the elemental composition of the material. Comparative EDXRF analysis conducted before and after treatment provided critical insights into changes in the adsorbent's physical and chemical properties. Both SEM and EDXRF analyses were performed in the Nanotechnology Laboratory. In addition, Fourier Transform Infrared Spectroscopy (FTIR) was applied to investigate the chemical characteristics of the adsorbent. Unlike EDXRF, which identifies elemental composition, FTIR detects functional groups and molecular structures through vibrational mode analysis, thereby offering essential information on adsorption mechanism.

Numerical simulation and data analysis

In this research, the removal efficiency of phosphorus was employed as the primary indicator for evaluating the performance of raw hard clam shells as a natural adsorbent in an up-flow column reactor treating synthetic phosphorus-containing water. Removal efficiency was determined by measuring the difference between influent and effluent phosphate concentrations over time. During operation, synthetic water with a predetermined initial phosphate concentration was passed through the columns packed with raw hard clam shells, and effluent samples were collected at specific time intervals. Phosphate concentrations in both influent (C_i) and effluent (C_e) were quantified using standard spectrophotometric methods. The adsorption effectiveness was subsequently expressed as the percentage of phosphate removed at each sampling point, calculated according to Equation (2).

$$E = \frac{C_i - C_e}{C_i} \times 100\% \quad (2)$$

where E represents the removal efficiency in percentage, C_i is influent phosphate concentration

(mg/L) and C_e is effluent phosphate concentration at a given time (mg/L).

Bed-Depth Service Time (BDST) model

The BDST model assumes that service time is directly proportional to the bed depth and inversely proportional to the influent concentration, assuming that adsorption follows first-order reaction. This model is particularly valuable for laboratory-scale experiments to industrial applications, as ot facilitates the prediction of the required bed depth for a given service time and influent concentration. The BDST relationship can be expressed in the form of a linear equation, as presented in Equation (3).

$$t = a \times e^{(b \times h)} \quad (3)$$

Equation (3) models the relationship between an adsorption column's service time (t) and its bed height (h). In this context, the service time represents the duration the column operates effectively before requiring maintenance or replacement. At the same time, the bed height refers to the vertical depth of the adsorbent material in the column. Parameters serve as the scaling factor, adjusting the overall impact of bed height on service time, and b are dimensionless constants that dictate the rate of exponential change. If $b>0$, the service time increases exponentially with bed height, indicating that taller columns provide longer operational times due to the increased adsorbent material available for interaction. Conversely, if $b<0$, service time decreases exponentially, which might occur in cases of inefficiencies at greater heights. This equation is beneficial for predicting the performance of an adsorption system and optimising bed height to achieve maximum operational efficiency and cost-effectiveness.

$$N_o = a \times C_o \times v \quad (4)$$

As in Equation (4), N_o represents the dynamic adsorption capacity per unit volume of the up-flow column reactor, measured in mg/L. This parameter quantifies the amount of phosphorus (PO_4^{3-}) that can be adsorbed per unit volume of the adsorbent, under dynamic flow conditions. Slope a (with unit h/cm) is a key factor that relates the bed height of the column to the service time, indicating how changes in bed height influence the overall adsorption performance. The influent phosphorus concentration, C_o (mg/L), is a critical factor affecting the adsorption capacity, as higher concentrations typically require more adsorbent material or longer contact times for effective removal. Lastly, v, the flow velocity (cm/h), determines the residence time of the phosphorus-laden water within the column. A slower velocity allows for more extended interaction between the phosphorus and the adsorbent, enhancing adsorption efficiency, while higher velocities may lead to reduced contact time and lower adsorption performance. Together, these parameters provide a comprehensive framework for designing and optimising adsorption columns for effective phosphorus removal.

$$K_a = \frac{1}{b \times Co} ln\left(\frac{C_o}{C_s} - 1\right) \quad (5)$$

As seen in Equation (5), the adsorption rate constant (K_a) is a critical parameter in adsorption studies, representing the speed at which phosphorus (PO_4^{3-}) is adsorbed onto the surface of the adsorbent. Measured in L h^{-1} mg^{-1}, K_a quantifies the rate at which adsorption occurs relative to the phosphorus concentration in the solution. The influent phosphorus concentration (C_o), expressed in mg L^{-1}, significantly influences the adsorption dynamics, as higher initial concentrations generally lead to increased adsorption rates initially but may saturate the adsorbent over time. The b-value, a dimensionless constant representing the y-intercept, reflects an intrinsic property of the system, such as initial conditions or system-specific factors that affect adsorption performance. These parameters help describe the kinetics and efficiency of phosphorus removal in adsorption systems, guiding the optimisation of operational conditions for effective treatment.

Thomas model

The Thomas model provides a simplified representation of the adsorption process by incorporating several key assumptions. It presumes that adsorption kinetics follow a Langmuir-type isotherm, with negligible axial dispersion. Furthermore, the model assumes that adsorption is a reversible, second-order reaction, where the rate is directly proportional to the number of available adsorption sites. The primary application of the Thomas model is in predicting breakthrough curves, which indicate the point at which the adsorbent in the column becomes saturated and effluent concentrations reach a critical level. Breakthrough time is a fundamental design parameter, as it defines the operational lifespan of the adsorbent and determines when regeneration or replacement is required. The Thomas model is expressed in Equation (6) [13].

$$\frac{Cs}{Co} = \frac{1}{1 + exp[KT(qo \times m - Co \times V) / Q]} \quad (6)$$

Where the Thomas rate constant (K_T) is measured in mL/mg.min quantifies the rate at which phosphorus (PO_4^{3-}) is adsorbed onto the adsorbent material, in this case, raw hard clam shells, under continuous flow conditions. The equilibrium phosphate uptake (q_o), expressed in mg/g, represents the maximum amount of phosphate adsorbed per gram of clam shell at equilibrium.

The adsorbent mass (m, in grams) within the column

directly affects the total adsorption capacity, as larger quantities provide more surface area for phosphorus removal. The synthetic water volume (V, in litres) corresponds to the effective volume of synthetic influent passing through the column, while the volumetric flow rate (Q, in L/h), determines the hydraulic contact time between the adsorbent and the aqueous phase. Higher flow rates reduce residence time and potentially lower adsorption efficiency, while a lower flow rates extended contact, thereby enhancing phosphate removal. Collectively, these parameters form the operational framework for evaluating and optimizing adsorption performance in continuous flow systems as expressed in Equation (7).

$$\ln(\frac{Co}{Cs} - 1) = -(c \times t) + d \quad (7)$$

With $c = K_T \times C_o$ representing the slope is a constant (h^{-1}), while $t = \frac{V}{Q}$ denotes the service time (h). The term $d = \frac{Kt \times qo \times m}{Q}$ corresponds to the y-intercept, a constant (dimensionless) as the experiment was conducted at a constant flow rate. The values of K_T and q_o can thus be determined for a given flow rate once the slope, c, and intercept, d, have been obtained from the linear graph of $\ln(C_O/C_S-1)$ against time, t.

This equation can be utilised to generate breakthrough curves, which offer insights into the point at which the adsorbent becomes saturated and can no longer effectively remove the adsorbate from the solution. The simplicity of this model enables its application in various continuous adsorption processes, encompassing water treatment, air purification, and industrial wastewater management. The Thomas model is useful for optimising operational parameters, including bed depth, flow rate, and influent concentration. By adjusting these parameters, engineers can anticipate the operational lifespan of the column before the breakthrough and enhance its efficiency.

The Modified Mass Transfer Factor (MMTF) model accounts for multiple resistances to mass transfer, including external film diffusion, intraparticle diffusion, and surface adsorption, thereby offering a more comprehensive description of adsorbate transport from the liquid phase to the adsorbent surface. This model is particularly useful in systems where adsorption is simultaneously influenced by surface interactions and the rate of solute transfer from the bulk solution into the pore structure of the adsorbent. The MMTF model integrates adsorption data commonly derived from equilibrium isotherm such as Langmuir or Freundlich, which describe the relationship between the solute concentration of adsorbate in solution and the amount adsorbed on the solid phase. By incorporating mass transfer limitations, the MMTF model enhances the accuracy of adsorption rate prediction, particularly under conditions where operational parameters such as flow rate and particle size strongly affect the adsorption process. The mathematical representation of the MMTF model is provided in Equation (8).

$$ln\left[ln\left(\frac{C_O}{C_S}\right)\right] = ln\left[[k_L a]_g \times \left(e^{-\beta q}\right) \times t\right] \quad (8)$$

$$ln\left[ln\left(\frac{C_O}{C_S}\right)\right] = ln\,[k_L a]_g + ln\left(e^{-\beta q}\right) + ln\,t$$

$$\beta q = ln\,[k_L a]_g - ln\left[ln\left(\frac{C_O}{C_S}\right)\right] + ln\,t$$

$$q = \frac{ln\,[k_L a]_g - ln\left[ln\left(\frac{C_O}{C_S}\right)\right] + ln\,t}{\beta}$$

Let $B = \frac{ln\,[k_L a]_g - ln\left[ln\left(\frac{C_O}{C_S}\right)\right] + ln\,t}{\beta}$, therefore q can be written as Equation (9)

$$q = B + \frac{1}{\beta} \times ln(t) \quad (9)$$

The equation $ln\left[ln\left(\frac{C_O}{C_S}\right)\right] = ln\left[[k_L a]_g \times \left(e^{-\beta q}\right) \times t\right]$ relates the concentration ratio of the influent (C_O) and effluent (C_S) to the Lag adsorption rate constant $[k_L a]_g$, the adsorption capacity (q), and time (t). Expanding it, write $ln\left[ln\left(\frac{C_O}{C_S}\right)\right] = ln\,[k_L a]_g + ln\left(e^{-\beta q}\right) + ln\,t$. Rearranging to isolate q, $q = \frac{ln\,[k_L a]_g - ln\left[ln\left(\frac{C_O}{C_S}\right)\right] + ln\,t}{\beta}$. Introducing B, where $let\ B = \frac{ln\,[k_L a]_g - ln\left[ln\left(\frac{C_O}{C_S}\right)\right] + ln\,t}{\beta}$, simplifies the equation further as $q = B + \frac{1}{\beta} \times ln(t)$. This highlights that q depends on a constant B and the logarithmic function of time $ln\,(t)$. The equation derivation for MMTF is shown in Equations (10) and (11).

$$ln\left(\frac{C_O}{C_S}\right) = [k_L a]_g \times e^{(-\beta \times ln(q)} \times t \quad (10)$$

$$ln\left[ln\left(\frac{C_O}{C_S}\right)\right] = ln\left[[k_L a]_g \times (e^{(-\beta \times ln(q)}) + t\right]$$

$$ln\left[ln\left(\frac{C_O}{C_S}\right)\right] = ln\,[k_L a]_g + \ln\,(e^{(-\beta \times ln(q)}) + ln\,(t)$$

$$ln(q) = \frac{ln\,[k_L a]_g - ln\left[ln\left(\frac{C_O}{C_S}\right)\right] + ln\,(t)}{\beta}$$

Let $B = \frac{ln\,[k_L a]_g - ln\left[ln\left(\frac{C_O}{C_S}\right)\right]}{\beta}$, therefore $ln(q)$ can be written as Equation (11)

$$ln(q) = B + \frac{1}{\beta} \times ln(t) \quad (11)$$

The given equation models the adsorption process in a system. Starting with $ln\left(\frac{C_O}{C_S}\right) = [k_L a]_g \times e^{(-\beta \times ln(q)} \times t$, it can be written as $ln\left[ln\left(\frac{C_O}{C_S}\right)\right] = ln\,[k_L a]_g + ln\,(e^{(-\beta \times ln(q))}) + ln\,(t)$. Simplifying further, $ln\,(q)$ is the natural log of adsorption capacity which is expressed as $ln(q) = \frac{ln\,[k_L a]_g - ln\left[ln\left(\frac{C_O}{C_S}\right)\right] + ln\,(t)}{\beta}$. By defining $let\ B = \frac{ln\,[k_L a]_g - ln\left[ln\left(\frac{C_O}{C_S}\right)\right]}{\beta}$, the equation simplifies to $ln(q) = B + \frac{1}{\beta} \times ln(t)$. This shows that $ln\,(q)$ is linearly dependent on $ln\,(q)$, with B representing a constant influenced by system parameters like $[k_L a]_g$and the concentration ratio $ln\left[ln\left(\frac{C_O}{C_S}\right)\right]$. In this model, the adsorption rate is determined by both external mass transfer, characterised by the film mass transfer coefficient, and the adsorption equilibrium, characterised by the discrepancy between the bulk and equilibrium concentrations. The MMTF model surpasses a mere depiction of the adsorbent's capacity by assessing the speed and efficiency of transferring the adsorbate from the solution to the adsorbent. This assessment is vital for the design of efficient column systems in practical applications.

Numerical simulation and data analysis

Physical and chemical characteristics of the raw hard clam shell adsorbent

The raw shell adsorbent possesses distinctive physical and chemical properties that enhance its effectiveness as a natural adsorbent material. Fourier Transform Infrared Spectroscopy (FTIR) analysis typically reveals functional groups, such as carbonates and hydroxyls, which provide active sites critical for contaminant interaction adsorption processes [14]. Scanning Electron Microscopy (SEM) observations show that the surface of the shell is rough and porous, thereby offering an extensive surface area that enhances adsorption capacity [15]. Elemental composition analysis using Energy Dispersive X-ray Fluorescence (EDXRF) confirms calcium as the predominant element, consistent with the shell's primary composition of calcium carbonate ($CaCO_3$), along with trace amounts of other elements such as magnesium, silicon, or strontium, contingent upon the shell's origin. X-ray Diffraction (XRD) patterns further verify the crystalline nature of the material, with calcite as predominant mineral phase, although polymorphs such as aragonite may also be detected. Taken together, these characteristics – presence of functional groups, porous morphology, high calcium content, and crystalline mineral phases – highlight the potential of raw clam shells as a promising candidate for adsorption-based environment applications [16].

The FTIR spectra of raw and phosphate (PO_4^{3-}) adsorbed hard clam shells (refer to **Figure 2**) were recorded over the range of 4000–400 cm^{-1} to examine alterations in surface functional groups before and after adsorption. As shown in **Table 2**, the comparison of the FTIR peaks reveals slight shifts and the appearance of new adsorption peaks following adsorption, indicating specific interactions between the phosphate ions and the functional groups present on the shell surface. Prior to adsorption of PO_4^{3-}, the FTIR spectrum of raw hard clam shell exhibited distinct bands at 1471.42 cm^{-1}, 896.63 cm^{-1}, and 860.95 cm^{-1}, characteristic of carbonate and related functional groups. These bands are associated with C–H bending, vinyl C–H bending, and C–O–O stretching vibrations, respectively, and align with the carbonate-based composition of the clam shell matrix, which is primarily calcium carbonate ($CaCO_3$). After exposure to the phosphate solution, the FTIR spectrum displayed minor shifts in these peaks to 1471.08 cm^{-1}, 895.24 cm^{-1}, and 859.96 cm^{-1}, indicating modifications in the bonding environment of the corresponding functional groups due to adsorption. These changes likely result from surface complexation between PO_4^{3-} and the Ca^{2+} or carbonate groups on the shell surface, forming phosphate-calcium complexes. Furthermore, new peaks appeared at 735.94 cm^{-1}, 712.55 cm^{-1}, and 676.31 cm^{-1} after adsorption. These newly detected bands are attributed to C–I and C–H bending vibrations, and their emergence further supports the conclusion that phosphate adsorption alters the chemical environment of the shell surface.

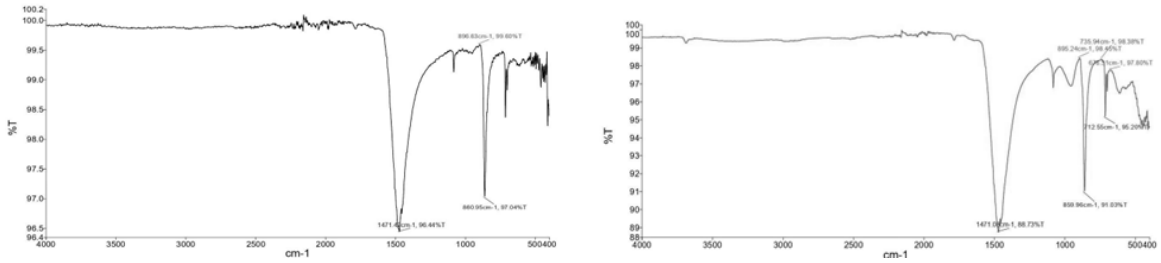

(a) (b)

Figure 2. FTIR spectra of adsorbent (a) before adsorption and (b) after adsorption of phosphorus (PO_4^{-3})

Table 2. FTIR spectra analysis before and after adsorption of PO_4^{-3} ions

Frequency Spectrum (cm^{-1})			Functional Group Indication	Reference
Before Adsorption	**After Adsorption**	**Difference**		
1471.42	1471.08	-0.37	C-H bend	[16]
896.63	895.24	-1.39	Vinyl C-H bend	[16]
860.95	859.96	-0.99	C-O-O stretch	[16]
-	735.94	-	C-I stretch	[16]
-	712.55	-	C-I stretch	[16]
-	676.31	-	C-H bend	[16]

The SEM analysis presented in **Figure 3** illustrates distinct morphological changes on the surface of raw hard clam shells before and after phosphorus adsorption. Prior to adsorption (refer to **Figures 3(a)** & **(b)**), the shell surface appeared relatively smooth, with well-defined crystalline features and a naturally layered structure, indicating inherent porosity without the presence of foreign deposits. Following phosphorus adsorption (refer to **Figures 3(c)** & **(d)**), the surface exhibited increased roughness and the formation of irregular, particle-like deposits, suggesting the precipitation of calcium phosphate compounds resulting from interactions between phosphate ions and calcium from the shell surface [17]. Although the specific surface area and pore size distribution were not quantified using BET analysis in this study, the observed porous and rough surface morphology is conducive to adsorption processes. Consistent with previous report on calcium carbonate-based shell materials, effective phosphate removal can occur despite relatively low to moderate surface areas, as the dominant removal mechanism are governed by surface precipitation and calcium-phosphate complexation rather than surface area alone. Nevertheless, future investigations will incorporate BET analysis to provide a more comprehensive evaluation of the adsorbent's textural properties.

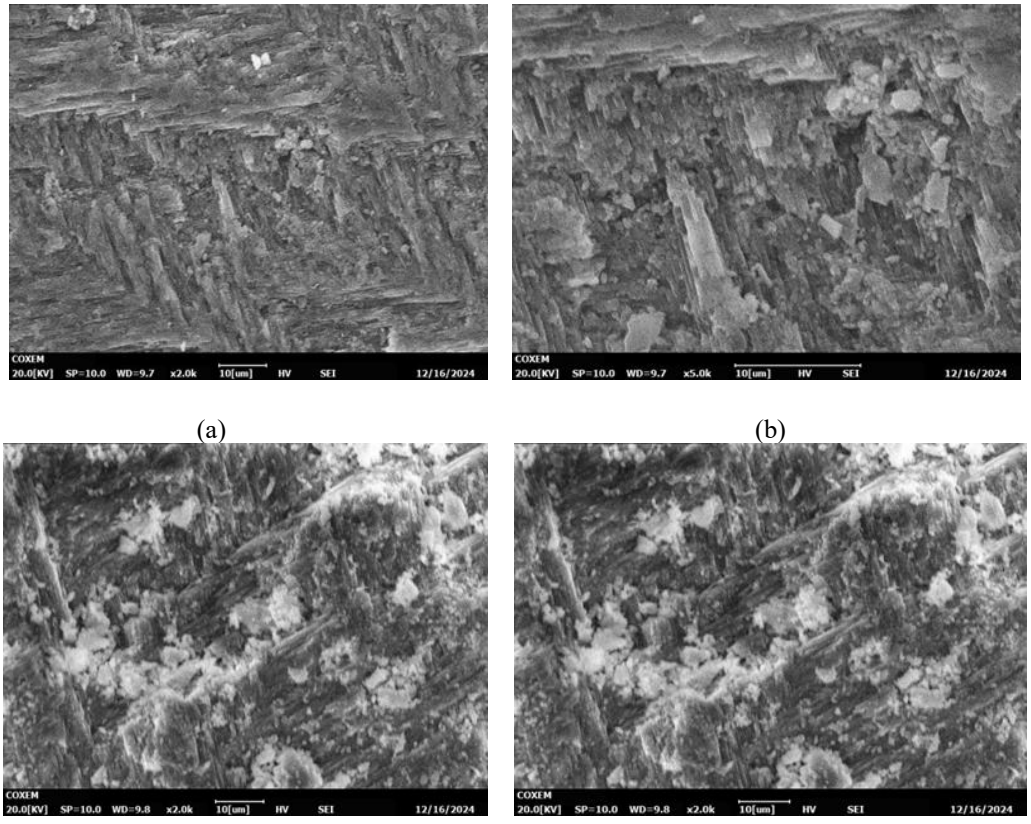

(a) (b)

(c) (d)

Figure 3. Surface morphology of the adsorbent before: (a) at 2000x magnification (b) at 5000x magnification, after: (c) at 2000x magnification (d) at 5000x magnification

The chemical composition of the adsorbent before and after the phosphate adsorption process was determined using the EDXRF test, and the results are presented in **Table 3**. The test identified elements including Ca, O, C, Al, Sr, Mg, and Na in the hard clam shell, along with their atomic weights per hard clam shell molecule. The highest percentages were found for Ca and O. The adsorption process was indicated by an increase in the atomic weight of Ca (from 38.42% to 41.28%) and a decrease in the atomic weight of O (from 52.37% to 45.67%) after adsorption, as showed in Table 3. The increase in Al content after adsorption (0.00% to 0.36%) is attributed to trace mineral impurities inherently present within the shell matrix or background interference during EDXRF analysis. In contrast, C showed an increased atomic weight (from 8.08% to 12.32%) following adsorption. This increase is likely attributed to the formation of carbonate ions, CO_3^{2-}, which remain on the adsorbent surface [18]. The increase in calcium content after adsorption is consistent with findings from other studies, which indicate that calcium-containing materials exhibit improved phosphate adsorption abilities due to surface reactions involving calcium [19]. The absence of detectable phosphorus is likely due to its low surface loading and limited sensitivity of EDXRF for light elements at low concentrations. Similar observations have been reported in shell-based adsorption systems where phosphorus removal occurs predominantly through surface precipitation rather than elemental accumulation detectable by EDX [17].

The X-ray diffraction (XRD) analysis reveals that before phosphorus adsorption, the raw hard clam shell predominantly consists of aragonite (83%) and sodium nitrate (17%), as illustrated in **Figure 4(a)**. Aragonite, a type of calcium carbonate ($CaCO_3$) derived from marine sources, dissolves more readily than calcite, making it effective for adsorption. Although sodium nitrate contributes soluble salts, its role in phosphorus removal is minimal. The high carbonate content of the shells, especially aragonite, makes them a suitable material for adsorption, providing a surface for phosphate binding and facilitating some ion exchange [20]. After adsorption, the composition of the shells changes significantly, as shown in **Figure 4(b)**. The proportion of aragonite decreases to 52%, while calcium carbonate increases to 39%, indicating a structural transformation. A new compound, manganese-magnesium-potassium oxide hydrate (9%), emerges in a nanocrystalline form, suggesting the occurrence of chemical reactions. These oxides enhance phosphorus uptake through surface binding and ion exchange, particularly involving magnesium and manganese, which may form insoluble phosphates. Over time, hydrolysis and recrystallisation could further modify the structure of the shells. The formation of new phases, such as insoluble phosphates or metal oxides, frequently occurs when shells are exposed to solutions containing metal ions or phosphates. This process enhances adsorption through surface binding and ion exchange, particularly with magnesium and manganese, which form stable, insoluble phosphates [21].

Performance of the up-flow column reactor system and its operating conditions

Figure 5(a) illustrates the phosphorus removal efficiency of PO_4^{-3} over time for different bed depths in the UFCR treatment system. The results indicate that shallower beds (1 cm and 2 cm) exhibit rapid saturation, leading to a swift decline in efficiency. The 1 cm bed commences with low removal efficiency and becomes ineffective within 60 hours, while the 2 cm bed initially removes approximately 16-17% of phosphorus but reaches 0% efficiency by around 120 hours. The 3 cm bed performs slightly better, with an initial efficiency of 20-25%, yet still saturates within 144-168 hours, as evidenced by the effluent phosphorus concentration approaching the influent value. As bed depth increases, removal efficiency improves significantly. The 4 cm bed begins at approximately 27-30% efficiency and maintains over 10% efficiency for about 120 hours before gradually declining to 0% between 174-198 hours. The 6 cm bed demonstrates even greater performance, initially achieving 30-35% efficiency and sustaining removal for approximately 200 hours before reaching saturation at around 243 hours. The most favourable performance is observed in the 8 cm bed, which commences with nearly 40% removal efficiency and remains above 20% for over 150 hours. Even after 216-243 hours, it exhibits some removal capacity, ultimately reaching complete saturation at approximately 300 hours.

Figure 5(b) illustrates the gradual saturation of the adsorption medium in an up-flow column reactor, demonstrating a decrease in phosphorus removal efficiency over time. Initially, at lower accumulation times, the final concentration (C_f) is significantly lower than the influent concentration (C_i = 10 mg/L), indicating effective phosphorus removal. The variation in C_f across different depths suggests that the deeper sections of the column retain their removal capacity for a longer period compared to the shallower sections. At shallower depths (e.g., 1 cm and 2 cm), C_f rises sharply, approaching the influent concentration within the first 100 hours. This indicates that the adsorption sites at these depths become saturated rapidly, resulting in a decline in phosphorus removal efficiency. As time progresses, phosphorus begins to break through in the deeper sections of the up-flow column reactor, as evidenced by the gradual increase in C_f at depths of 3 cm, 4 cm, 6 cm, and 8 cm. The deeper layers, particularly at 6 cm and 8 cm, exhibit a more sustained removal capacity, with C_f increasing at a slower rate than in the shallower depths. By approximately 174 to 198 hours, the column shows signs of approaching saturation at most depths, which

represent points where C_f reaches or nears 10 mg/L. Beyond 200 hours, the up-flow column reactor's capacity to remove phosphorus diminishes significantly, with all depths displaying C_f values close to C_i, signalling complete exhaustion of adsorption sites. This trend confirms that the deeper layers enhance phosphorus retention, thereby prolonging the up-flow column reactor's effective lifespan before complete breakthrough occurs [22].

Table 3. The EDXRF spectrometer analysed the chemical composition of raw hard clam shell material

Element	Weight (%)	
	Before adsorption	**After adsorption**
Ca	38.42	41.28
O	52.37	45.67
C	8.08	12.32
Al	0.00	0.36
Sr	0.36	0.37
Mg	0.00	0.00
Na	0.77	0.00
Total	100.00	100.00

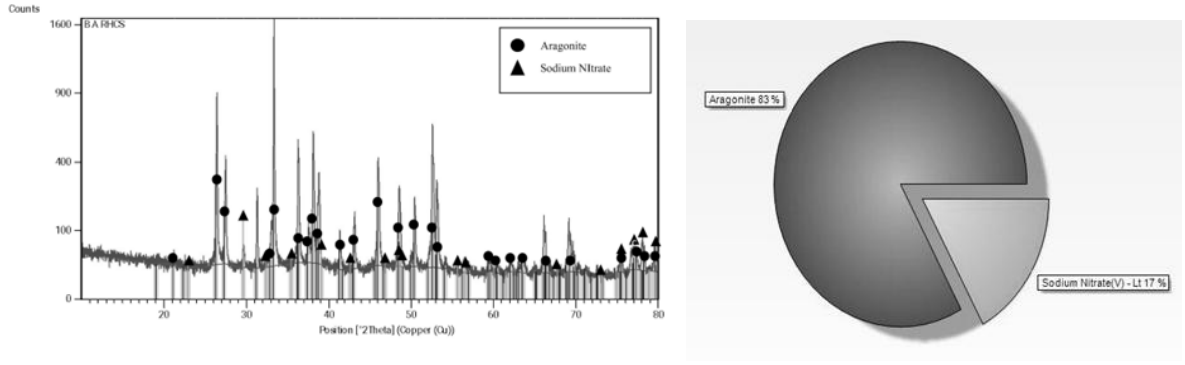

(a)

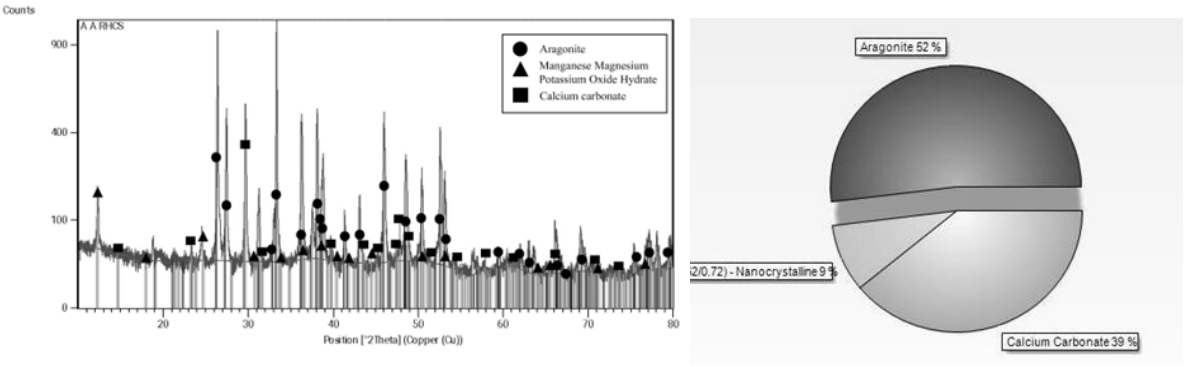

(b)

Figure 4. XRD spectra of aragonite and sodium nitrate components of the adsorbent (a) before adsorption and (b) after adsorption

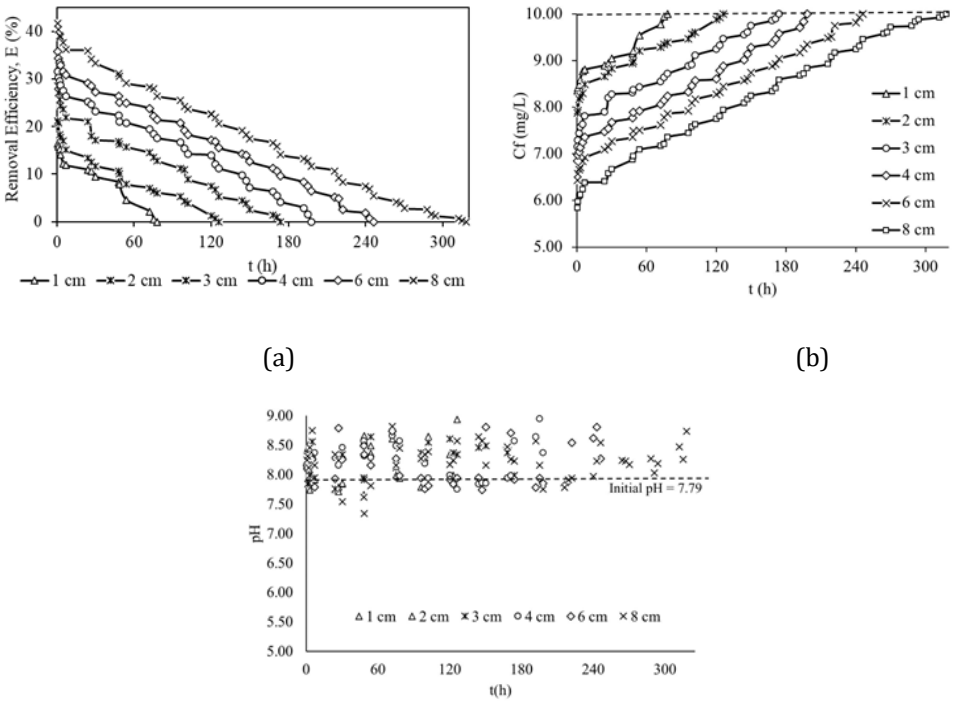

Figure 5. The performance of (a) removal efficiency, E (%), (b) Final concentration, Cf (mg/L), (c) pH, against t (h) for every bed height

Based on **Figure 5(c)**, pH was measured at six different depths (1 cm, 2 cm, 3 cm, 4 cm, 6 cm, and 8 cm) over an extended period. The influent solution initially exhibited a pH of 7.79, as indicated by the dashed line in the figure. As synthetic water traversed the up-flow column reactor, pH values generally increased, suggesting that the raw hard clam shells contributed to the alkalinity. The variations in pH at different depths imply that the dissolution of calcium carbonate ($CaCO_3$) from the raw hard clam shell affected pH differently, contingent upon contact time and reaction dynamics. At lower depths (1 cm to 3 cm), the pH was slightly elevated during the early hours of the experiment, where pH values at these depths often exceeded 8.0. This can be attributed to the rapid dissolution of calcium carbonate upon initial contact with the influent. The dissolution releases calcium ions and carbonate ions (CO_3^{2-}), which neutralise hydrogen ions and subsequently raise pH [23]. However, at these shallow depths, the influent has limited contact time with the raw hard clam shell, which may result in less effective phosphorus adsorption. As the solution progresses further into the column, intermediate depths (4 cm to 6 cm) exhibit more stable pH values, typically ranging from 7.9 to 8.5, suggesting that the up-flow column reactor system is approaching a state of equilibrium. This stabilisation indicates that the release of calcium ions has reached a balance, optimising conditions for phosphorus precipitation. The presence of Ca^{2+} ions facilitate the formation of calcium phosphate ($Ca_3(PO_4)_2$), a key mechanism for phosphorus removal. At greater depths (6 cm to 8 cm), pH trends remain relatively stable; slight fluctuations indicate ongoing reactions. The results indicate that pH at these depths generally remains above the influent pH but does not significantly exceed the levels observed at intermediate depths. This suggests that most available Ca^{2+} ions have already reacted, diminishing alkalinity contributions. Figure 5(c) illustrates this phenomenon, as pH values at later time points tend to cluster around a stabilised range. This indicates that phosphorus removal is likely at its peak efficiency in these deeper sections of the column. The performance of the up-flow column reactor system is closely linked to the physical-chemical properties of the raw hard clam shell adsorbent and its operating conditions. Raw hard clam shells, which are rich in calcium carbonate (aragonite), possess a porous surface and active functional groups that facilitate phosphate adsorption through surface complexation and precipitation of calcium phosphate. Analyses using FTIR, SEM, EDXRF, and XRD confirmed the occurrence of chemical interactions, increased calcium content, and structural changes after adsorption. Greater bed depths (6 – 8 cm) improved removal efficiency and prolonged adsorption capacity due to increased contact time, while higher pH levels, resulting from the dissolution of $CaCO_3$, further enhanced phosphate removal. These findings demonstrate how the properties of the

adsorbent and the design of the reactor work together to optimise phosphorus removal [24].

Bed Depth Service Time Model analysis

The adsorption performance was evaluated over time intervals ranging from 0 minutes up to 1800 minutes (30 hours). Effluent phosphate concentration increased progressively from 0 mg/L at the onset to a maximum of 10.00 mg/L by the end of the experiment. Sampling intervals were initially set at 0.5 minutes to capture rapid early-stage dynamics and later adjusted to 30 minutes as the process stabilized. At the beginning of the experiment, the adsorbent demonstrated strong phosphate retention, reflected in a low effluent concentration. With extended operation, however, the adsorption sites became saturated, resulting in gradual rise in effluent phosphate levels. Application of the BDST model indicated the relationship between service time and bed depth follows a linear trend, where a higher bed depth extends the adsorption capacity. The breakthrough point, where phosphate concentration reached a significant portion of its initial value, was observed at around 4320 minutes (4 days) with an effluent concentration of approximately 10 mg/L. Beyond this point, the system approached exhaustion, as indicated by the concentration rising steadily towards 10 mg/L [25]. The data confirms the applicability of the BDST model in predicting adsorption performance, which can be used for scale-up calculations in continuous column adsorption systems.

The adsorption performance of phosphate onto raw marsh clam shell was evaluated using the Bed Depth Service Time (BDST) model to estimate the dynamic adsorption capacity (N_0) and adsorption rate constant (Ka) under varying breakthrough conditions. The BDST model assumes plug flow behaviour pattern with negligible axial dispersion and is commonly employed to describe the relationship between bed depth (h) and service time (t) prior to column saturation. According to the linearised BDST equation, $t = a \times e^{(b \times h)}$, where $a = \frac{No}{Co.v}$ and $b = \frac{1}{Ka.Co} \ln\left(\frac{Co}{Cs} - 1\right)$, the slope, a and intercept, b are extracted from the plot of service time versus bed depth. In this study, the breakthrough curves were generated for various effluent to influent concentration ratios (C_s/C_o) at 85%, 89%, 94%, 96%, and 99%, as shown in **Figures 6 (a – e)**. The regression equations and fitted lines demonstrated varying linearity, with coefficients of determination (R^2) increasing from 0.669 at 85% breakthrough to 0.907 at 99%, indicating that the BDST model better describes the system at higher degrees of column saturation. As the breakthrough concentration increased, a consistent rise in slope a was observed from 3.640 h/cm at 85% to 81.112 h/cm at 99% indicating that longer service times are achievable with deeper beds at higher breakthrough thresholds. Correspondingly, the dynamic adsorption capacity N_o also increased substantially, from 1,433.12 mg/L at 85% to 31,936.75 mg/L at 99%, suggesting more phosphate was retained within the column at higher levels of bed utilisation. This trend confirms the capacity of the clam shell media to maintain adsorption performance over extended operational periods and under greater contaminant loading. The increasing N_o values are consistent with enhanced packing and utilisation of the adsorbent bed at higher effluent concentrations.

Interestingly, according to **Table 4**, the adsorption rate constant K_a values were negative across all conditions and became increasingly negative with higher breakthrough percentages, decreasing from –0.299 L/mgh at 85% to –2.543 L/mgh at 99%. These negative values indicate a rapid change in the breakthrough profile and suggest deviation from ideal BDST assumptions, likely due to increasing mass transfer resistance or limitations in pore diffusion as the bed becomes saturated. Such behaviour is commonly observed in packed-bed adsorption systems, where external film diffusion and internal pore diffusion limit access to active adsorption sites, particularly at higher solute phosphate concentrations [26, 27]. Overall, the BDST model provided valuable insights into the scaling behaviour of the column and helped quantify the influence of bed depth on service time. The results underscore that phosphate adsorption is highly dependent on both operational depth and breakthrough concentration, and that raw clam shell exhibits favourable characteristics for use in column adsorption systems. The increase in N_o and improvement in R^2 values at higher C_s/C_o ratios support the application of this model for preliminary design, although refinement using more advanced models that account for mass transfer limitations (such as the Thomas or MMTF models) is recommended for more precise predictions under non ideal flow conditions.

Table 4. Analysis of the use of BDST models for the adsorption of PO_4^{3-} onto Raw Hard Clam Shell

C_s/C_o (%)	a (h cm^{-1})	b (dimensionless)	R^2	N_o (mg L^{-1})	K_a (L h^{-1} mg^{-1})
85	3.640	0.580	0.669	1433.122	-0.299
89	26.687	0.297	0.825	10507.645	-0.704
94	54.826	0.212	0.864	21586.996	-1.297
96	65.589	0.197	0.883	25824.782	-1.610
99	81.112	0.181	0.907	31936.753	-2.543

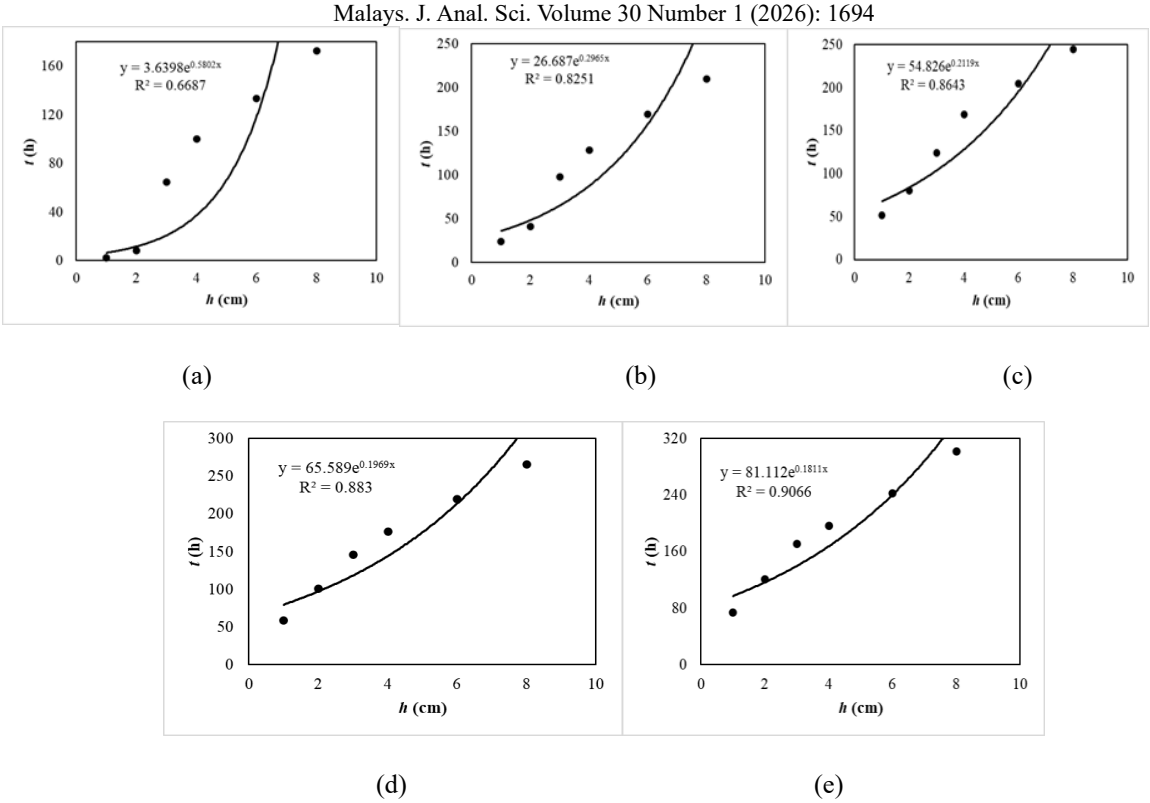

Figure 6. The linear curves of plotting C_s/C_o (%) for (a) 85, (b) 89, (c) 94, (d) 96, and (e) 99

Thomas Model analysis

The kinetic of phosphate (PO_4^{-3}) adsorption onto raw hard clam shell adsorbent were evaluated using the Thomas Model, based on the data obtained at a fixed flow rate of 0.1933 L h−1 across various depths of the up-flow column reactor. A linear plot of $\ln(C_o/C_s-1)$ versus time (refer to Figure 7) derived from Equation (6), results in a linear graph with the slope, c and the Y-intercept, d values, which were subsequently used to calculate the Thomas rate constant, K_T and adsorption capacity, q_o. Strong correlation were observed for the parameters K_T and q_o is robust ($R^2 > 0.904$; refer to Table 5), confirming that the model adequately describes the kinetic behaviour of phosphate adsorption onto the clam shell surface. The result showed a sequential decrease K_T from 0.0033 to 0.0022 to 0.0017 to 0.0013 and ultimately to 0.0012 L h^{-1} mg^{-1}, and in q_o from -0.0116 to -0.0077 to -0.0043 to -0.0034 to -0.0016 and -0.0001 mg g^{-1} as bed depth increased from 1 cm to 8 cm, as shown in **Table 5**.

The collision frequency of PO_4^{-3} ions with the acceptor sites of $CaCO_3$ polymorphs diminished as the dosage of granular raw hard clam shell increased, as evidenced by the reduced K_T value for a given flow rate of synthetic water passing through the up-flow column reactor bed according to XRD analysis (Refer **Figure 4**). Furthermore, the distribution of PO_4^{-3} ions across the raw hard clam shell adsorbent can expand with more raw hard clam shells in the up-flow column reactor bed, enabling it to retain a substantial quantity of PO_4^{-3} ions deposited on its surface. The kinetic coefficient, K_T decreased with the reduction in water velocity, which results from increased raw hard clam shell dosage; this sensitivity is associated with the pore space characteristics of raw hard clam shell, influenced by its internal structure and the chemical functional groups of the acceptor sites [26]. The observed decrease in q_o with increasing up-flow column reactor depth may be attributed to a diminishing driving force for the transport of PO_4^{-3} ions from the bulk liquid to the film zone near the solid surface, a phenomenon exacerbated by a larger quantity of the raw hard clam shell adsorbent [27]. Applying the Thomas models for PO_4^{-3} adsorption can elucidate the collision frequency and driving force of mass transfer, which pertains to the external mass transfer of PO_4^{-3} from the bulk liquid to the solid surface of the raw hard clam shell adsorbent.

Modified Mass Transfer Factor Model analysis

The Modified Mass Transfer Factor (MMTF) model was applied to evaluate adsorption behaviour of phosphorus at bed heights ranging from 1 to 8 cm. The model parameters, β and B were obtained through linear regression, with the corresponding coefficient of determination (R^2) presented in Table 6. The β values decreased from 1.005 to 0.800 g·h·mg^{-1} as bed height increased, indicating a reduction in the overall mass transfer rate with thicker adsorbent layers. In contrast, the B values exhibited a progressively negative trend, ranging from -2.510 to -3.900 mg.g^{-1},

suggesting enhance adsorption capacity at greater bed depth. All regression analysis produced R^2 values above 0.99, indicating an excellent model fit and validating the applicability of the MMTF model in describing phosphorus adsorption dynamics undervarying column depths.

To further investigate the adsorption kinetics and transport characteristics in the up-flow column reactor system, we analysed the mass transfer coefficients: the global mass transfer coefficient $[k_L a]_g$, the film mass transfer coefficient $[k_L a]_f$, and the diffusional mass transfer coefficient $[k_L a]_d$. These coefficients were examined in relation to the percentage of outflow and bed height. Figure 8(b) illustrates the variation of $[k_L a]_g$ with the percentage of outflow for all tested bed heights. The values of $[k_L a]_g$ exhibited a declining trend as the outflow percentage increased, indicating a reduction in the global mass transfer rate as the system approached saturation. This trend was more pronounced in shorter bed heights (e.g., h = 1 cm and 2 cm), where the limited mass transfer area resulted in faster breakthrough and earlier saturation. In contrast, higher bed heights (e.g., h = 6 cm and 8 cm) maintained higher $[k_L a]_g$ values for longer periods, signifying enhanced dispersion and increased contact time. The global mass transfer coefficient $[k_L a]_g$, calculated using Equation (9), was significantly affected by the ratio of the initial phosphorus concentration (C_O) to the equilibrium concentration (C_s). The parameters β and B have been validated through linear regression analysis. When plotted against the percentage of phosphate (PO_4^{3-}) breakthrough (see Figure 6a), $[k_L a]_g$ showed a clear decreasing trend with increasing outflow, indicating a diminishing mass transfer rate of phosphate ions from synthetic water to the reactive sites on the raw hard clam shell. This reduction is due to the weakened van der Waals and electrostatic forces as the pore spaces of the shell became occupied by phosphate and other ions. Additionally, the decrease in $[k_L a]_g$ with column depth underscores the escalating driving force needed for phosphate ions to reach the reactive surfaces of calcium ions (Ca^{2+}). Increased flow through the up-flow column reactor enhances interactions between phosphate anions and reactive sites. To optimise phosphate removal efficiency in this system, a detailed analysis of phosphate adsorption's mass transfer dynamics is crucial. Understanding whether the mass transfer rate is governed by film mass transfer or pore diffusion will provide essential insights for improving performance and addressing environmental concerns [3].

Table 5. The parameters K_T and q_o using the Thomas models

h (cm)	m (mg)	K_T (L h^{-1} mg^{-1})	q_o (mg g^{-1})	R^2
1	7785.0	0.0033	-0.0116	0.762
2	15341.0	0.0022	-0.0077	0.880
3	23751.0	0.0017	-0.0043	0.904
4	31835.0	0.0013	-0.0034	0.902
6	45269.0	0.0012	-0.0016	0.855
8	63316.0	0.0012	-0.0001	0.850

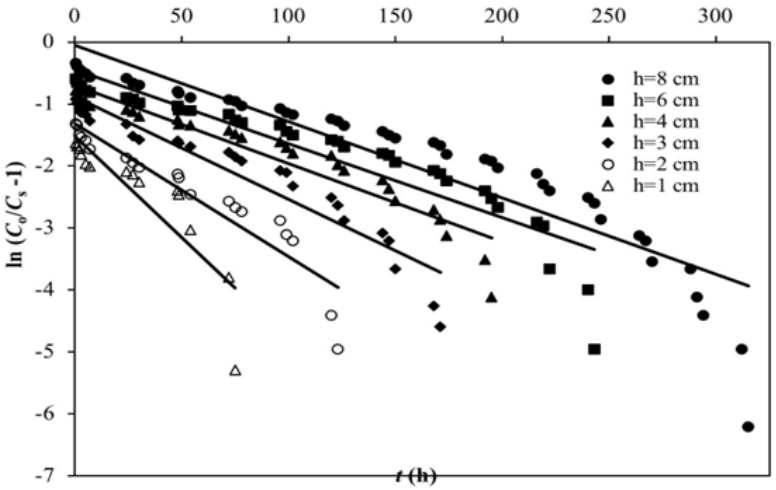

Figure 7. The linear curves of plotting $\ln(C_o/C_s - 1)$ versus t(h)

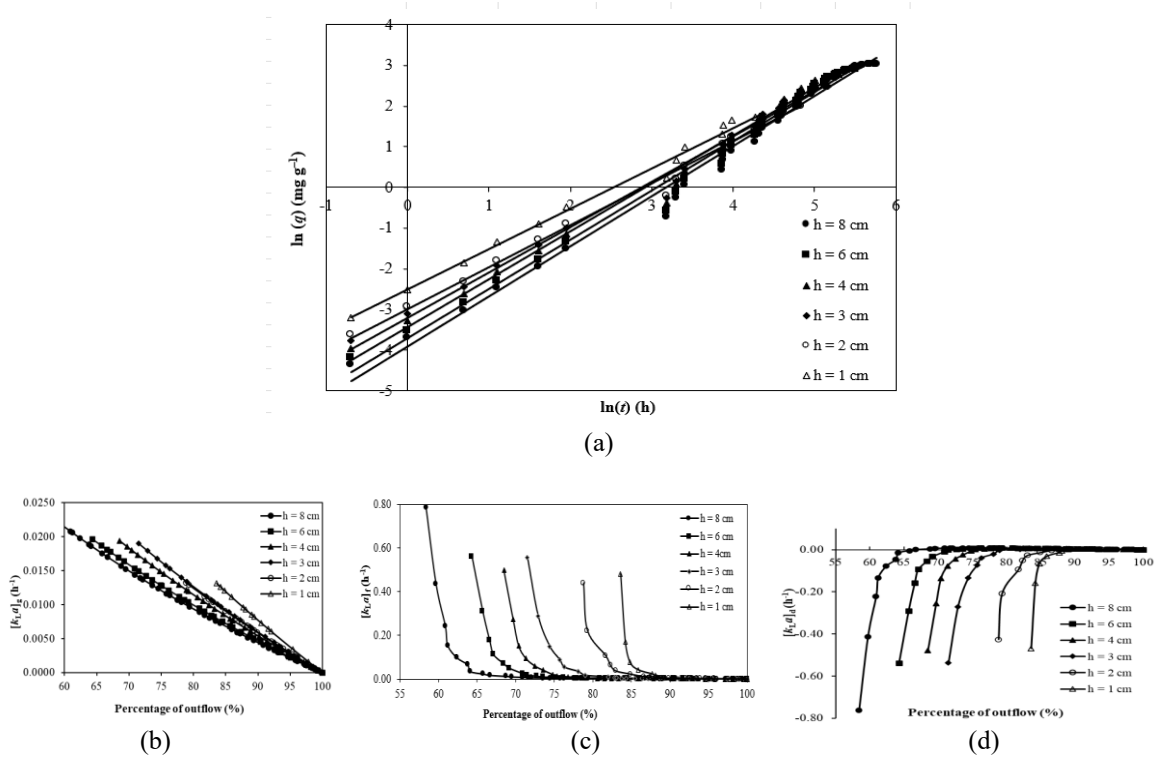

Figure 8. Modified mass transfer factor models (MMTF), (a) Logarithmic Breakthrough Curve at Various Bed Depths, (b) The global mass transfer coefficient $[k_L a]_g$ (c) The film mass transfer coefficient $[k_L a]_f$ and (d) The diffusional mass transfer coefficient $[k_L a]_d$

Figure 8(c) presents the behaviour of $[k_L a]_f$, which is primarily associated with the boundary layer or film resistance around the adsorbent particles. The values showed a sharp decline in the early stages of outflow, especially in shorter columns, indicating high initial driving forces and rapid adsorption. For taller beds, the decline in $[k_L a]_f$ occurred more gradually, suggesting a more sustained film diffusion mechanism due to a larger number of active sites and increased residence time. The film mass transfer coefficient $[k_L a]_f$, indicates the rate at which phosphate ions (PO_4^{3-}) cross the hydrodynamic boundary layer surrounding raw hard clam shell particles, essential for assessing external mass transfer efficiency in fixed-bed adsorption systems. A higher $[k_L a]_f$, suggests better ion transfer and enhanced adsorption performance. **Figure 8(c)** shows how $[k_L a]_f$, changes with phosphate breakthrough percentage, highlighting an initial sharp decline before 5% breakthrough. This decline reflects strong electrostatic attractions between the negatively charged phosphate ions and positively charged adsorption sites on the clam shell, driven by calcium ions (Ca^{2+}). Early-stage reactions involve forming insoluble calcium phosphate compounds, particularly under alkaline conditions where hydroxide ions (OH^-) lead to hydroxyapatite formation, as described in the following chemical reaction:

$5Ca^{2+} + 3PO_4^{3-} + OH^- \rightarrow Ca_5(PO_4)_3(OH)(s)$ [28].

Figure 8(d) displays the trend of $[k_L a]_d$, which reflects the internal diffusion resistance within the adsorbent material. At early stages (60–75% outflow), the values of $[k_L a]_d$ were significantly higher, particularly in shorter beds, but declined quickly as adsorption reached equilibrium. In taller columns, $[k_L a]_d$ values remained relatively stable, indicating that intraparticle diffusion played a more dominant role in the overall adsorption process and contributed to prolonged performance. The pore diffusion mass transfer coefficient $[k_L a]_d$ measures the rate at which phosphate ions (PO_4^{3-}) diffuse through the pore structure of the raw hard clam shell. While $[k_L a]_f$ governs transport across the external boundary layer, $[k_L a]_d$ describes internal mass transfer resistance, especially in porous materials, where adsorption occurs both on the surface and within the pore network. Figure 8(d) shows that $[k_L a]_d$ decreases as phosphate breakthrough progresses, indicating a reduced rate of intraparticle diffusion over time. This decline is mainly due to pore saturation and blockage from accumulated phosphate ions and coexisting anions. As phosphate occupies internal pore spaces, effective diffusivity decreases due to reduced porosity and increased diffusion path length. Additionally, chemical reactions involving naturally present calcium ions (Ca^{2+}) may lead to the formation of

Table 6. The parameter Modified mass transfer factor models (MMTF)

h (cm)	$\beta\ (g\ h\ mg^{-1})$	$B\ (mg\ g^{-1})$	R^2
1	1.005	-2.510	0.9929
2	0.966	-2.990	0.9932
3	0.897	-3.199	0.9916
4	0.819	-3.623	0.9905
6	0.800	-3.891	0.9909
8	0.813	-3.900	0.9906

hydroxyapatite minerals within the pores, further hindering diffusion. Overall, the trends in $[k_La]_g$, $[k_La]_f$, and $[k_La]_d$ provide complementary insights into the multi-phase mass transfer mechanisms occurring within the packed bed. The data collectively suggest that increasing bed height improves overall adsorption efficiency by enhancing contact time and promoting both external and internal mass transfer. These findings reinforce the applicability of the Modified Mass Transfer Function model and validate the design approach for optimising column operation for phosphorus removal.

Conclusion

This study demonstrates the potential of raw hard clam shells as a low cost and sustainable adsorbent for phosphate (PO_4^{3-}) removal from the synthetic water in an up-flow column reactor. Continuous operation showed that a bed depth of 8 cm achieved the highest and most stable removal performance, with approximately 40% phosphate removal maintained for over 300 hours. Although the removal efficiency under synthetic condition was moderate, these findings establish a clear baseline performance for an unmodified natural adsorbent and confirm its technical viability in continuous-flow systems. Material characterisation (FTIR, SEM, EDXRF, and XRD) confirmed phosphate uptake through surface and structural changes, including the formation of calcium phosphate compounds. Column modelling using the Bed Depth Service Time, Thomas, and Modified Mass Transfer Factor models provided consistent interpretation of the system behaviour. The BDST model indicated that deeper beds enhance dynamic adsorption capacity, the negative K_a values suggested complex kinetics. The Thomas model indicated that phosphate transport efficiency decreased with increasing bed height, and the MMTF model emphasised that pore diffusion was the main mass transfer mechanism. All models showed strong agreement with experimental data ($R^2 > 0.99$). In conclusion, raw hard clam shells show promise as an environmentally sustainable adsorbent for phosphate removal in continuous treatment systems. Further improvement through adsorbent modification, regeneration strategies, and validation using real wastewater are required prior to large-scale implementation.

Acknowledgement

This research was supported by Universiti Tun Hussein Onn Malaysia (UTHM) through Tier 1 (Vot J133) and Geran Penyelidikan Pascasiswazah, GPPS (Vot Q673).

References

1. Wu, K., Li, Y., Liu, T., Huang, Q., Yang, S., Wang, W., & Jin, P. (2019). The simultaneous adsorption of nitrate and phosphate by an organic-modified aluminum-manganese bimetal oxide: Adsorption properties and mechanisms. *Applied Surface Science*, 478, 539-551.
2. Li, R., Wang, J. J., Zhou, B., Awasthi, M. K., Ali, A., Zhang, Z., & Mahar, A. (2016). Enhancing phosphate adsorption by Mg/Al layered double hydroxide functionalized biochar with different Mg/Al ratios. *Science of the Total Environment*, 559, 121-129.
3. Fulazzaky, M. A., Khamidun, M. H., Din, M. F. M., & Yusoff, A. R. M. (2014). Adsorption of phosphate from domestic wastewater treatment plant effluent onto the laterites in a hydrodynamic column. *Chemical Engineering Journal*, 258, 10-17.
4. Osman, N. A., Ujang, F. A., Roslan, A. M., Ibrahim, M. F., & Hassan, M. A. (2020). The effect of palm oil mill effluent final discharge on the characteristics of Pennisetum purpureum. *Scientific Reports*, 10(1), 6613.
5. Nagoya, S., Nakamichi, S., & Kawase, Y. (2019). Mechanisms of phosphate removal from aqueous solution by zero-valent iron: A novel kinetic model for electrostatic adsorption, surface complexation and precipitation of phosphate under oxic conditions. *Separation and Purification Technology*, 218, 120-129.
6. Lalley, J., Han, C., Li, X., Dionysiou, D. D., & Nadagouda, M. N. (2016). Phosphate adsorption using modified iron oxide-based sorbents in lake water: kinetics, equilibrium, and column tests. *Chemical Engineering Journal*, 284, 1386-1396.
7. De Gisi, S., Lofrano, G., Grassi, M., & Notarnicola, M. (2016). Characteristics and adsorption capacities of low-cost sorbents for wastewater treatment: A review. *Sustainable Materials and Technologies*, 9, 10-40.

8. Zhang, Z., Yan, L., Yu, H., Yan, T., & Li, X. (2019). Adsorption of phosphate from aqueous solution by vegetable biochar/layered double oxides: fast removal and mechanistic studies. *Bioresource Technology*, 284, 65-71.
9. Mezenner, N. Y., & Bensmaili, A. (2009). Kinetics and thermodynamic study of phosphate adsorption on iron hydroxide-eggshell waste. *Chemical Engineering Journal*, 147(2-3), 87-96.
10. Liu, S., Sun, Y., Wang, R., Mishra, S. B., Duan, H., & Qu, H. (2018). Modification of sand with iron and copper derived from electroplating wastewater for efficient adsorption of phosphorus from aqueous solutions: A combinatorial approach for an effective waste minimization. *Journal of Cleaner Production*, 200, 471-477.
11. Fulazzaky, M. A., Salim, N. A. A., Puteh, M. H., Khamidun, M. H., Yusoff, A. R. M., Fulazzaky, M., ... & Zaini, M. A. A. (2022). Reliability of the mass transfer factor models to describe the adsorption of NH^{4+} by granular activated carbon. *International Journal of Environmental Research*, 16(3), 30.
12. Mekonnen, D. T., Alemayehu, E., & Lennartz, B. (2021). Fixed-bed column technique for the removal of phosphate from water using leftover coal. *Materials*, 14(19), 5466.
13. Khadhri, N., Saad, M. E. K., ben Mosbah, M., & Moussaoui, Y. (2019). Batch and continuous column adsorption of indigo carmine onto activated carbon derived from date palm petiole. *Journal of Environmental Chemical Engineering*, 7(1), 102775.
14. Yusuf, M. O. (2023). Bond characterization in cementitious material binders using Fourier-transform infrared spectroscopy. *Applied Sciences*, 13(5), 3353.
15. Goldstein, J. I., Newbury, D. E., Michael, J. R., Ritchie, N. W., Scott, J. H. J., & Joy, D. C. (2017). Scanning electron microscopy and X-ray microanalysis. springer.
16. Nandiyanto, A. B. D., Oktiani, R., & Ragadhita, R. (2019). How to read and interpret FTIR spectroscope of organic material. *Indonesian Journal of Science and Technology*, 4(1), 97-118.
17. Onoda, H., Fukatsu, R., & Tafu, M. (2013). Reaction of sea shells with resemble phosphorus wastewater and application of products. *Journal of Environmental and Occupational Science*, 2(2), 71.
18. Janusz, W., & Sędłak, A. (2011). Specific adsorption of carbonate ions at the hematite/aqueous electrolyte solution interface. *Physicochem Probl Miner Process*, 46, 65-72.
19. Muslima, N. H., Faizalb, A. D. M., Sophianb, M. A. S., Abd Rashidb, M. A. F., Abdullahb, N. H., Hassana, N. A., & Salimd, N. A. A. (2025). Removal of phosphorus from water onto marsh clam shell to predict contour for removal efficiency and mass of adsorbent. *Jurnal Kejuruteraan*, 37(1), 309-321.
20. Zahed, M. A., Salehi, S., Tabari, Y., Farraji, H., Ataei-Kachooei, S., Zinatizadeh, A. A., ... & Mahjouri, M. (2022). Phosphorus removal and recovery: state of the science and challenges. *Environmental Science and Pollution Research*, 29(39), 58561-58589.
21. Nadagouda, M. N., Varshney, G., Varshney, V., & Hejase, C. A. (2024). Recent advances in technologies for phosphate removal and recovery: A review. *ACS environmental Au*, 4(6), 271-291.
22. Edahwati, L., Muryanto, S., Jamari, J., & Bayuseno, A. P. (2017). Use of upflow fluidized bed reactor (fbr) for recovery phosphorus from waste-water through struvite precipitation. *Advanced Science Letters*, 23(12), 12263-12267.
23. Lei, Y., Narsing, S., Saakes, M., Van Der Weijden, R. D., & Buisman, C. J. (2019). Calcium carbonate packed electrochemical precipitation column: new concept of phosphate removal and recovery. *Environmental Science & Technology*, 53(18), 10774-10780.
24. Khan, M. D., Chottitisupawong, T., Vu, H. H., Ahn, J. W., & Kim, G. M. (2020). Removal of phosphorus from an aqueous solution by nanocalcium hydroxide derived from waste bivalve seashells: mechanism and kinetics. *ACS omega*, 5(21), 12290-12301.
25. Shin, C. W., Son, S. K., Lee, Y., Kim, S. K., Jin, H. G., Lee, D. W., & Ahn, M. Y. (2023). Experimental validation of bed depth service time model using vapor adsorption bed for coolant purification system of fusion research. *Fusion Engineering and Design*, 192, 113716.
26. Ahmed, M. J., & Hameed, B. H. (2018). Removal of emerging pharmaceutical contaminants by adsorption in a fixed-bed column: a review. *Ecotoxicology and Environmental Safety*, 149, 257-266.
27. Charola, S., Yadav, R., Das, P., & Maiti, S. (2018). Fixed-bed adsorption of Reactive Orange 84 dye onto activated carbon prepared from empty cotton flower agro-waste. *Sustainable Environment Research*, 28(6), 298-308.
28. Ferro, A. C., Seixas, T., & Guedes, M. (2024). Reaction path in the mechanosynthesis of calcium phosphates using a biogenic calcium source. *Ceramics International*, 50(1), 282-292.